International Journal of Microwave and Wireless Technologies, 2009, 1(5), 403–413.
doi:10.1017/S175907870999050X

A compact semi-lumped tunable complex-impedance transformer

ANNE-LAURE PERRIER[1,*], JEAN-MARC DUCHAMP[2], OLIVIER EXSHAW[2,†], ROBERT HARRISON[3] AND PHILIPPE FERRARI[2]

This article describes the design and performance of a compact tunable impedance transformer. The structure is based on a transmission line loaded by varactor diodes. Using only two pairs of diodes, the circuit is very small with a total length of only λ/10. Both the frequency range and the load impedance can be tuned by varying the varactor bias voltages. Our design provides a tunable operating frequency range of ±40% and an impedance match ranging from 20 to 90 Ω at 0.8 GHz and from 30 to 170 Ω at 1.5 GHz. In addition, a new approach that considers losses for the simulation and measurement of this impedance transformer was investigated. The measured performance of a 1 GHz prototype design confirmed the validity of this new approach.

Keywords: Impedance transformer, Microwave, Miniaturized device, Tunable device, Varactors

Received 21 January 2009; Revised 24 August 2009; first published online 8 September 2009

I. INTRODUCTION

One of the most formidable challenges in the field of microwave telecommunications is designing tunable devices. In the near future, more and more applications will require systems that can operate over variable frequency ranges. Tunable impedance transformers are important in applications such as transistor impedance matching over a large tunable bandwidth for maximum gain or minimum noise factor purposes, in designing tunable power dividers, in characterizing Monolithic Microwave Integrated Circuit (MMIC) transistors, and in general matching networks.

Microwave impedance transformers and matching networks are based either on transmission-line sections having specific characteristic impedances, or on L, T, or Π structures. The most usual section type is the quarter-wave impedance transformer, while L, T, or Π structures can be realized by using lumped elements like CLC (capacitor–inductor–capacitor) devices [1], or by using single- or double-stub structures.

The overall length of transmission-line-based structures can be reduced by loading a high impedance line with capacitors [2]. Such devices can also be made tunable if the fixed capacitors are replaced by tunable capacitors, such as varactor diodes or Micro Electro Mechanical Systems (MEMS) capacitors.

[1]Laboratory of Microwaves and Characterization (LAHC), University of Savoie, 73376 Le Bourget-du-Lac, France. (Email: anne-laure.perrier@univ-lyon1.fr)
[2]Institute of Microelectronics, Electromagnetism and Photonics (IMEP), UMR 5130 CNRS, INPG-UJF, BP 257, 38016 Grenoble Cedex 1, France. (Emails: duchamp@minatec.inpg.fr; philippe.ferrari@ujf-grenoble.fr; Olivier.Exshaw@grenoble.cnrs.fr)
[3]Department of Electronics, Carleton University, Ottawa K1S 5B6, Canada. (Email: rgh@doe.carleton.ca)
*Present address: Université de Lyon, Creatis-LRMN, UMR 5220 CNRS, U630 Inserm, Lyon 1 University, INSA Lyon, 69616 Villeurbanne, France.
†Present address: Research Center for Very Low Temperatures (CRTBT), UPR 5001 CNRS, UJF-INPG, BP 166, 38042 Grenoble Cedex 9, France.
Corresponding author:
Anne-Laure Perrier
Email: anne-laure.perrier@univ-lyon1.fr

In the last decade, several authors have proposed the use of transmission lines loaded by switches in series or in parallel to realize tunable impedance transformers [3, 4, 5]. These first devices demonstrated the impedance transformer principle but they cover a small part of the Smith chart. Based on a CLC structure and a quarter-wave transformer, a resonant cell topology [6] has been used in several configurations [7, 8, 9]. In spite of a medium Smith chart coverage, the length of these devices is important because they are realized with a minimum of two quarter-wave transformers.

With the MEMS switches and MEMS varactors development, other designs based on single-stub [10], double-stub [11, 12, 13] or triple-stub topologies [14, 15] have also been realized. Most of these devices need lots of MEMS switches or varactors complicating the bias commands. Moreover, these impedance transformers require large surface to cover, in general, small or medium part of the Smith chart.

Lots of these impedance transformers are demonstrated to be used as tuners and some of them are used to realize antenna [9] or transistor [16] matching. Recently, new and improved tunable impedance transformers have been described. A very compact lumped-element CLC impedance transformer with a ±36% tunable bandwidth for a 50 Ω load was demonstrated [17]. Some designs, based on transmission lines with variable characteristic impedance, were also presented [18, 19]. These devices are original but not lead a large coverage of the Smith chart. A double-slug impedance tuner, based on a distributed MEMS transmission line and employing 80 RF-MEMs switches, could produce 1954 different complex impedances around the center of the Smith chart [20]. This device is also original but we note the important number of MEMS switches witch complicate the bias commands. A MEMS impedance tuner was realized at 25 GHz [21]. This design was used with MEMS varactors, and provided continuous impedance coverage. Compared to the other impedance transformers referenced in this paper, this MEMS impedance tuner is optimized in term of surface, variable element number, and Smith chart coverage.

Table 1 resumes the impedance transformers topology and performance. Lot of these examples required more than three varactors, complicating the circuit with numerous bias voltages. Those based on quarter-wave transmission lines result in physically long structures with narrow bandwidths.

Moreover, many of these designs were characterized only for a 50 Ω load, so that the insertion loss was known only for that particular case. In some instances, only S_{11} was measured, resulting in no information on insertion loss.

This article describes how a tunable and compact impedance transformer, using only two pairs of varactors, was designed. Two different methods for the optimization and experimental characterization of the circuit were developed. The first and the simplest method was based on the synthesized impedances representation with a 50 Ω load. In this case, the synthesized impedance was extracted from the S_{22} parameter. The insertion loss was not measured for complex loads.

The second method was much more complete: the return loss and the insertion loss of the transformer, loaded by a complex impedance, were calculated and measured using an external tuner. We emphasize that the first method is accurate only for lossless devices, as it cannot extract the characteristics of lossy circuits.

In a previous study [24, 25], we demonstrated the ability of a new topology to design a tunable complex-impedance transformer, operating at 5 GHz. Its length was ∼λ/3 and it needed only two varactors. Its key features were a large matching impedance range, from 5 to 300 Ω, and a tunable frequency range of ±15%. However, this prototype exhibited significant insertion loss, from 2 to 6 dB, owing to the use of low-Q varactors, resulting in a nonoptimized design.

This article describes the design and performance of a new, more compact, and better optimized configuration than the one presented earlier [24]. The design procedure leads to a small λ/10 long transformer with reduced insertion loss.

This article is organized into six sections. Section II details the principle of the impedance transformer. The transformations from 50 Ω to possible complex impedances are illustrated on Smith charts. Section III presents the development of two different simulation approaches: "synthesized impedance" method, and the "matching load" method. The two methods are compared in the case of lossy and lossless circuits. Section IV discusses the design of an impedance transformer

Table 1. Impedance transformers topology and performance.

Impedance transformer type + operating frequency	Variable capacitor	Technology	Dimensions	Smith chart coverage
Transmission line				
[3], 27 GHz	4 MIM capacitors + HEMT transistors	Monolithic, GaAs	1*1 mm², λ/5*λ/5	Very small, some complex impedances
[5], 18 GHz	8 pHEMT switches	Monolithic, GaAs	2.4*0.8 mm², λ/3*λ/9	Small, ≈50 complex impedances
[22], 20–50 GHz	8 MEMS switches	Monolithic, glass $\varepsilon_r = 4{,}6$	2.5*1 mm², λ/2*λ/5	Medium, 256 complex impedances
[20], 12–25 GHz	80 MEMS switches	Monolithic, quartz $\varepsilon_r = 3{,}8$	10 mm, λ	Medium, 1954 complex impedances
[21], 27–30 GHz	4 MEMS varactors + 1 MIM capacitor	Monolithic, Si	0.49*0.12 mm², λ/8*λ/30	Good, continuous
[23], 0.05–2 GHz	FET switches			Good, 36 complex impedances
[19], 0.9 GHz	2 varactors	Hybrid, Rogers $\varepsilon_r = 3$	30*30 mm², λ/8*λ/8	Small, continuous
[18], 2.14 GHz	p–i–n diode	Hybrid, RF35 $\varepsilon_r = 3{,}5$	λ/4	Very small, 50, 89, or 200 Ω
Resonant cell				
1 resonant cell [6], 2.4 GHz	3 varactors	Hybrid, Rogers TMM10i	λ/2	Continuous from 4 to 392 Ω, no complex impedances
2 resonant cells [7], 23 to 25 GHz	MEMS varactors	Monolithic, quartz	3.7*2 mm², λ/2*λ/4	Medium, continuous
1 resonant cell [9], 0.39 GHz	12 diodes p–i–n	Hybrid		Medium, 4096 complex impedances
Stub				
Double-stub [8], 29–32 GHz	12 MEMS switches	Monolithic, quartz	3*2 mm², λ/2*λ/3	Small, 49 complex impedances
Double-stub [11], 10–20 GHz	8 MEMS switches	Mixed, Si and alumina	≈3λ*2λ	Small
Double-stub [12], 10–20 GHz	8 MEMS switches	Mixed, Si and alumina	18*11 mm², 1.3λ*0.8λ	Small to good, 256 complex impedances
Double-stub [13], 10 GHz	6 MEMS switches	Monolithic, Si $\varepsilon_r = 11.7$	6*7 mm², λ/2*λ/2	Small, 64 complex impedances
Double-stub [16], 8–12 GHz	4 MEMS switches + 1 varactor	Monolithic		Small, (transistor matching)
Triple-stub [14], 6–20 GHz	11 MEMS switches	Monolithic, glass $\varepsilon_r = 4{,}6$	7.3*7.3 mm², λ/2*λ/2	Medium to very good
Single-stub [10], 20–50 GHz	10 MEMS switches	Monolithic, glass $\varepsilon_r = 4{,}6$	5.6*3.6 mm², λ*3λ/2	Good
Triple-stub [15], 4.5 GHz	5 varactors	Hybrid, duroid $\varepsilon_r = 6{,}15$	28 mm, λ	No measurement of complex impedances

https://doi.org/10.1017/S175907870999050X Published online by Cambridge University Press

for a proof of concept. This device is realized in a printed board hybrid technology. The simulated and measured results obtained by the two different methods are compared in Section V. Finally, Section VI contains concluding remarks.

II. PRINCIPLE

The equivalent electrical circuit of the complex-impedance transformer is shown in Fig. 1. Its total electrical length is θ, and it consists of three transmission-line sections of equal characteristic impedance Z_c, and different electrical lengths θ_1, θ_2, and θ_3. The transmission line is loaded by two tunable capacitors C_{v1} and C_{v2}.

Assuming that the electrical length θ_i ($i = 1, 2,$ or 3) of each section is small as compared to the electrical wavelength ($\lambda^\circ = 2\pi$), a section can be replaced by its lumped-element equivalent circuit, as shown in Fig. 2(b). The characteristic impedance Z_c and phase velocity v_φ of the transmission line are defined thus

$$Z_c = \sqrt{\frac{L}{C}} \quad \text{and} \quad v_\varphi = \frac{1}{\sqrt{LC}}, \tag{1}$$

where L is the inductance and C the capacitance per unit length of the transmission line.

From the lumped equivalent circuit of a section (see Fig. 2(b)), Z_{ci} and $v_{\varphi\iota}$ can also be expressed thus

$$Z_{ci} = \sqrt{\frac{L_i'}{C_i' + C_{vi}}} \quad \text{and} \quad v_{\varphi i} = \frac{l_i}{\sqrt{L_i'(C_i' + C_{vi})}}, \tag{2}$$

where $L_i' = Ll_i$ and $C_i' = Cl_i$. The quantities, L_i' is the equivalent inductance and C_i' the equivalent capacitance of a section of physical length l_i:

$$l_i = \frac{\theta_i}{2\pi f} \frac{c}{\sqrt{\varepsilon_{r_{eff}}}}, \tag{3}$$

where c is the light celerity and $\varepsilon_{r_{eff}}$ the effective dielectric constant.

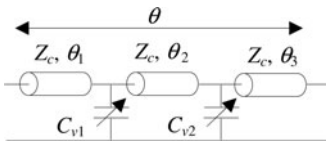

Fig. 1. Equivalent electrical circuit of the impedance transformer.

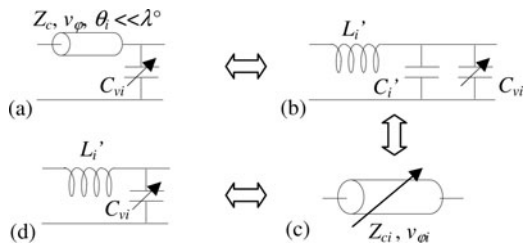

Fig. 2. Equivalent circuits of one section of the impedance transformer.

Each section of the impedance transformer is equivalent to a transmission line with a tunable characteristic impedance Z_{ci} and phase velocity $v_{\varphi i}$ (see Fig. 2(c)). The maximum tunability of Z_{ci} and $v_{\varphi i}$ was obtained when $C_i' \ll C_{vi}$. This condition was satisfied when Z_c was large, leading to the simplified equivalent electrical circuit of Fig. 2(d).

If Z_c is large and if the total electrical length θ is small as compared to the wavelength, the equivalent circuit of the complex-impedance transformer can be simplified, as shown in Fig. 3. This simplified equivalent electrical circuit will be used to explain the principle of the complex-impedance transformer. Each section has now been replaced by its equivalent inductance L_i'. The quantities Z_{L1}, Z_{LC1}, Z_{L2}, Z_{LC2}, and Z_{out} are the output impedances as seen at different transverse planes indicated by the dotted lines, when the input port is terminated by 50 Ω. The Smith charts of Fig. 4 show the principle of all the impedance transformations, starting from the 50-Ω input port in (a) to the output impedance Z_{out} in (e). These transformations assume a fixed frequency and no losses. In the impedance chart of Fig. 4(a), one can see that the

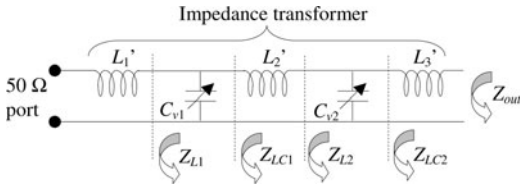

Fig. 3. Simplified equivalent electrical circuit of the complex-impedance transformer.

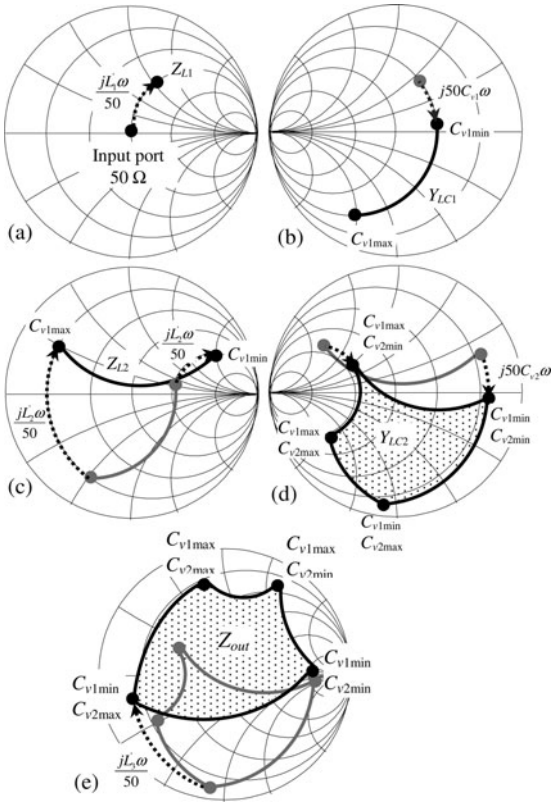

Fig. 4. Principle of impedance transformations. The impedances (a) Z_L1, (b) $Z_{LC}1$, (c) Z_L2, (d) $Z_{LC}2$, and (e) Z_{out} are synthesized at the transverse planes of the impedance transformer, as shown in Fig. 3.

https://doi.org/10.1017/S175907870999050X Published online by Cambridge University Press

inductance L_1' transforms the 50 Ω input impedance to Z_{L1} at the output end of inductor L_1'. In the admittance chart of Fig. 4(b), it can be seen that the variable capacitive admittance ωC_{v1} transforms Z_{L1} to a range of admittances Y_{LC1}. The Y_{LC1} output admittance values are part of the circle defined by $\omega C_{v1\min}$ and $\omega C_{v1\max}$, where $C_{v1\min}$ and $C_{v1\max}$ are the minimum and maximum capacitance values. A second $L'C_v$ section is necessary to transform this circular arc into a surface, as shown in the impedance and admittance charts (Figs 4(c) and 4(d)). The final inductance L_3' allows the achievable Z_{out} area on the Smith chart to be rotated. This area corresponds to a value of S_{22} when the output is terminated by 50 Ω.

III. OPTIMIZATION METHOD

The Smith charts given in Section II show that the Z_{out} impedance area depends on the three inductances L_1', L_2', and L_3', the minimum and maximum values $C_{\min}$ and $C_{\max}$ of the two capacitors, and the operating frequency f. All these parameters need to be optimized according to the tuner application. In this section we develop and compare two different methods for optimizing an impedance transformer. The first method is based on the display of the Z_{out} area (see Fig. 4(e)) using the S_{22} parameter for a 50 Ω load. Examples of synthesized impedances obtained by this method are shown in Subsection IIIA below. The second method calculates the S_{11} and S_{21} parameters when the impedance transformer is loaded with complex impedances. The principle of this "matching load" method is given in Subsection IIIB. In Subsection IIIC we compare the two methods with a typical example. The comparison is made both by including and omitting the losses to determine their effect on the second optimization method.

In practice, not all the elements constituting the impedance transformer are ideal. In the optimization process, the complete equivalent electrical circuit of a commercial varactor diode (Fig. 5) was considered. M/A-COM™ varactors (MA4ST-1240) with a series inductance $L_s = 1.2$ nH, a series resistance $R_s = 1.6$ Ω, a case capacitance $C_c = 0.11$ pF, and a tunable capacitance $C(V)$ ranging from 1.5 to 8.6 pF were used. A single varactor was used to realize each tunable capacitor in Fig. 1. To compare the two approaches, we specified that the impedance transformer should have the parameters $Z_C =$ 200 Ω, $\theta_1 = 15^\circ$, $\theta_2 = 15^\circ$, and $\theta_3 = 8^\circ$. Ideal transmission lines were assumed for the simulations.

A) First approach: the "synthesized impedance" method

The first approach, the "synthesized impedance" method, is based on the display of the S_{22} parameter when the impedance transformer is loaded by 50 Ω. Many state of the art tuners are just characterized this way, and so insertion loss versus the load, is not known.

Figure 6 shows the synthesized impedances of the impedance transformer at (a) 0.5 GHz, (b) 1 GHz, and (c) 1.5 GHz. The thick lines correspond to a fixed minimum or maximum value for the capacitance of one varactor and a complete variation of the other. In some cases, this area is not sufficient to show all possible synthesized impedances. With intermediate values of the two capacitors, all the shaded area shown in Fig. 7 can be covered by this impedance transformer. The synthesized impedance area in Fig. 7(b) is larger than the area in Fig. 6(b). In this section, simulation results are shown as in Fig. 7. In Section V, measured results are presented as in Fig. 6.

B) Second approach: the "matching load" method

For the second method, the impedance transformer was loaded by complex impedance. The setup shown in Fig. 8 corresponds to a typical real working configuration of the transformer, for example when it is used as a matching network for a transistor. Here, the input return loss S_{11} and insertion loss S_{21} of the impedance transformer were investigated. In the following discussion, we refer to this approach as the "matching load" method.

The simulations were done by a Mathematica [26] program, developed to automatically calculate the Smith chart coverage for the entire range of varactor capacitances. A flowchart of the program is given in Fig. 9.

Figure 10 shows all the complex loads that were tested by the program. For each load, the cascade *ABCD* and *S* matrices

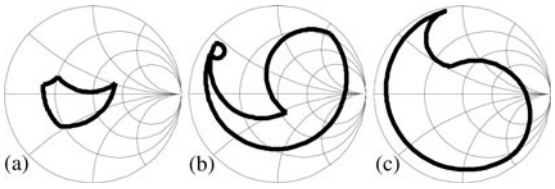

Fig. 6. Synthesized impedances at (a) 0.5 GHz, (b) 1 GHz, and (c) 1.5 GHz.

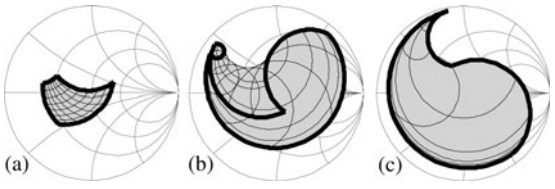

Fig. 7. Total area of the synthesized impedances at (a) 0.5 GHz, (b) 1 GHz, and (c) 1.5 GHz.

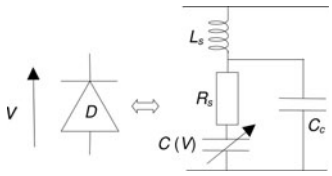

Fig. 5. Equivalent circuit of the reverse-biased varactor diode.

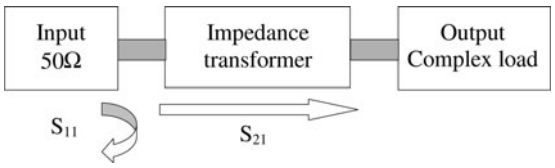

Fig. 8. Experimental setup for the measurement of S_{11} and S_{21}.

https://doi.org/10.1017/S175907870999050X Published online by Cambridge University Press

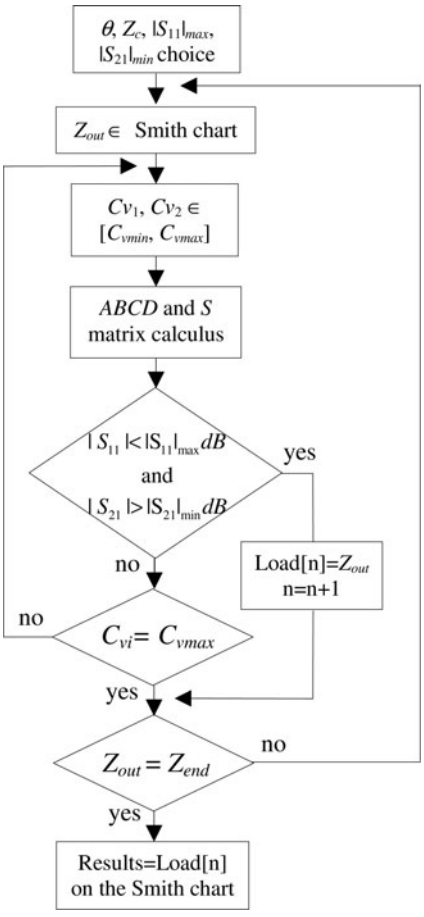

Fig. 9. Flowchart for the Mathematica simulation program.

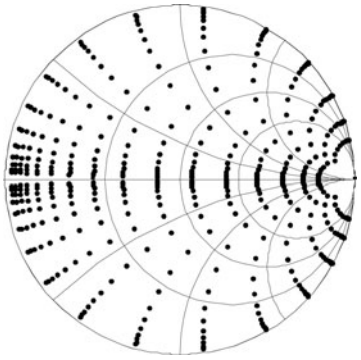

Fig. 10. Complex loads generated by the program.

of the impedance transformer were calculated, with two criteria $|S_{11}|_{\max}$ and $|S_{21}|_{\min}$ applied to the $|S_{11}|$ and $|S_{21}|$ parameters. The two capacitor values, C_{v1} and C_{v2} that satisfy the two criteria were extracted. Then the "matching load" area was plotted on the Smith chart. Equations for calculating S parameters in the case of a complex load are [27]:

$$S_{11} = \frac{AZ_{out} + B - CZ_{in}^{*}Z_{out} - DZ_{in}^{*}}{AZ_{out} + B + CZ_{in}Z_{out} + DZ_{in}}, \tag{4}$$

$$S_{12} = \frac{2(AD - BC)(\mathrm{Re}(Z_{in})\mathrm{Re}(Z_{out}))^{1/2}}{AZ_{out} + B + CZ_{in}Z_{out} + DZ_{in}}, \tag{5}$$

$$S_{21} = \frac{2(\mathrm{Re}(Z_{in})\mathrm{Re}(Z_{out}))^{1/2}}{AZ_{out} + B + CZ_{in}Z_{out} + DZ_{in}}, \tag{6}$$

$$S_{22} = \frac{-AZ_{out}^{*} + B - CZ_{in}Z_{out}^{*} + DZ_{in}}{AZ_{out} + B + CZ_{in}Z_{out} + DZ_{in}}, \tag{7}$$

where $\mathrm{Re}(Z_{in})$ and $\mathrm{Re}(Z_{out})$ are the real parts of the input and output impedances, respectively.

Comment: The simplified equivalent circuit of Fig. 3 is used in order to understand and easily visualize all the impedance transformations on the Smith chart. However, in the simulation process, for the "synthesized impedance" and "matching load" methods, we have compared equivalent electrical circuit of Figs 1 and 3 by using *ABCD* transmission-line matrix and *ABCD* inductance matrix, respectively. We have demonstrated that results are identical for small length impedance transformers and similar for longer devices. In this paper all the simulations shown in the figures have carried out with the equivalent electrical circuit of Fig. 1 i.e. with the used of real transmission lines.

C) Comparison between the two methods

In this subsection, simulation results of the impedance transformer obtained by the two different methods and described at the beginning of Section III are compared. Results are shown for the 1 GHz center frequency. In Sub-subsections 1), 2), and 3), the two methods are compared with the varactor R_s as a parameter. In Sub-subsection 4), we demonstrate that the results obtained when an impedance transformer was optimized using the "synthesized impedance" method, without considering losses, can be quite different from those obtained when the varactor losses were included.

1) LOSSLESS VARACTORS

In lossless microwave devices, the *S*-parameter moduli are related by

$$|S_{11}|^2 + |S_{21}|^2 = 1. \tag{8}$$

For a matching criterion $|S_{11}| < -20$ dB, relation (8) leads to $|S_{21}| > -0.04$ dB. With the criteria $|S_{11}|_{\max} = -20$ dB and $|S_{21}|_{\min} = -0.04$ dB, Fig. 11 shows the "conjugate synthesized impedances" and the "matching loads" obtained from the two

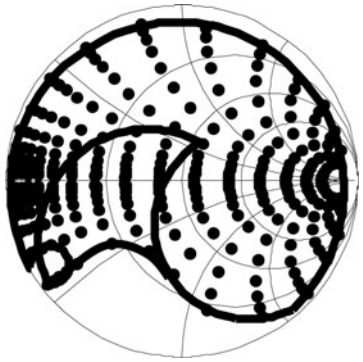

Fig. 11. Simulated coverage areas according to the "conjugate synthesized impedances ($S_{22}{}^{*}$)" approach (▬) and the "matching loads" approach (•••), at 1 GHz without varactor's series resistance, i.e., lossless varactors.

https://doi.org/10.1017/S175907870999050X Published online by Cambridge University Press

different methods. In this lossless case, the results of the two methods are perfectly superposed.

2) LOSSY VARACTORS

In this sub-subsection, the varactor series resistance R_s was considered. Figure 12 shows the results obtained from the two different methods when $|S_{11}|_{max} = -20$ dB, for several $|S_{21}|_{max}$ values. Because of R_s, the "matching load" method gives no possible loads when $|S_{21}|_{min} = -0.1$ dB; for $|S_{21}| < -2$ dB, the covered areas remain small. In this case, a perfect superposition of the results obtained by the two methods is never obtained. These results show that for lossy varactors, the "conjugate synthesized impedance" method, which is much simpler for experimental characterization, fails to give the correct covered area. Figure 12 proves the importance of the "matching load" method to know the insertion loss of the device versus this complex load. So, a 50 Ω measurement is not sufficient to characterize the tuner insertion loss.

For further simulations, the criterion $|S_{21}|_{min} = -2$ dB was applied.

3) INFLUENCE OF THE VARACTOR SERIES RESISTANCE R_S

In this sub-subsection the complex-impedance coverage was investigated by varying the series resistance R_s of the varactor as a parameter. Figure 13 compares the results obtained from the "synthesized impedance" and "matching load" methods, with $|S_{11}|_{max} = -20$ dB and $|S_{21}|_{min} = -2$ dB. For each Smith chart, the areas obtained by the two methods decrease as R_s increases.

The difference of area between the two methods increase with R_s so for a fixed complex load the insertion loss increases with R_s.

4) APPLICATION EXAMPLE

To investigate the impact of choosing the design method, an impedance transformer was designed to cover the largest possible area, while using the "synthesized impedance" method. The same MA4ST-1240 M/A-COM^{TM} varactor ($R_s = 1.6$ Ω) was used and the characteristic impedance of the line was also fixed to 200 Ω. The maximum "conjugate synthesized impedance" area was obtained when $\theta_1 = 40^\circ$, $\theta_2 = 15^\circ$, and

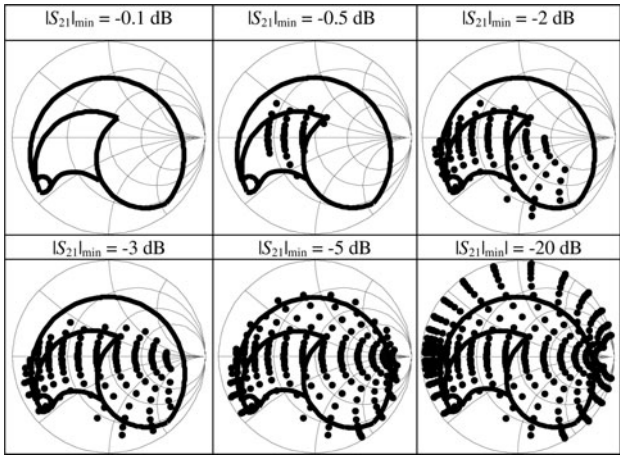

Fig. 12. Simulated coverage areas at 1 GHz according to the "conjugate synthesized impedance" (S_{22}^*) method (▬) and the "matching load" method (•••), when $R_s = 1.6$ Ω. Results are plotted for $|S_{21}|_{min}$ values from −0.1 to −20 dB.

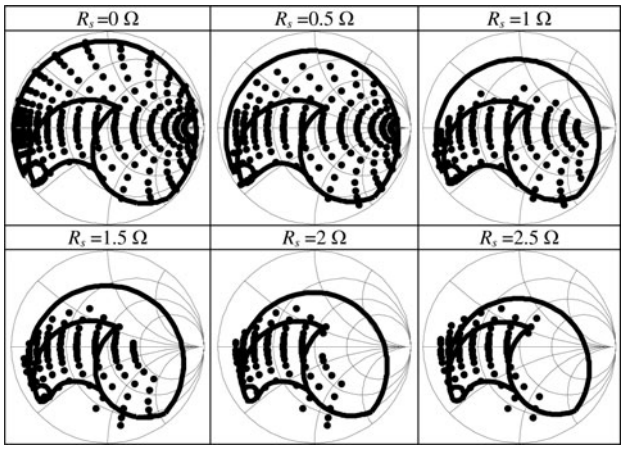

Fig. 13. Simulated 1 GHz coverage areas according to the "conjugate synthesized impedance" (S_{22}^*) method (▬) and the "matching load" method (•••). Here the varactor series resistance R_s is varied.

$\theta_3 = 8^\circ$. The same transformer was then simulated using the "matching load" method, with the criteria $|S_{11}| < -20$ dB and $|S_{21}| > -2$ dB. Results are compared in Fig. 14. A few loads allowing $|S_{11}| < -20$ dB and $|S_{21}| > -2$ dB were found at 1 GHz (see Fig. 14(a)), but no loads were found at 1.5 GHz (see Fig. 14(b)). However, a large area was obtained with the "conjugate synthesized impedance" method.

These typical results bring to the fore the importance of the design method. For lossy varactors the "synthesized impedance" method, which is used by several researchers in the field, can be very inaccurate because insertion loss information cannot be obtained.

The same impedance transformer ($\theta_1 = 40^\circ$, $\theta_2 = 15^\circ$, $\theta_3 = 8^\circ$, and $Z_c = 200$ Ω) was simulated by the two methods assuming $R_s = 0.5$ Ω (see Fig. 15). The covered areas of the "matching

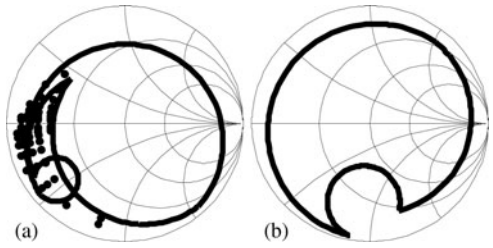

Fig. 14. Simulated coverage areas according to the "conjugate synthesized impedance" (S_{22}^*) method (▬) and the "matching load" method (•••), at (a) 1 GHz, and (b) 1.5 GHz for a 40°–15°–8° impedance transformer, with $R_s = 1.6$ Ω.

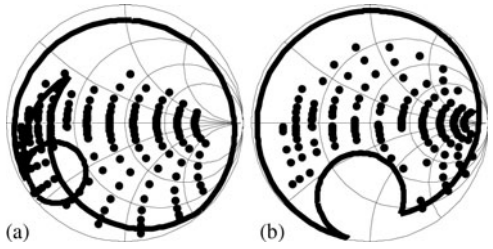

Fig. 15. Simulated coverage areas according to the "conjugate synthesized impedances" (S_{22}^*) method (▬) and the "matching load" method (•••), at (a) 1 GHz, and (b) 1.5 GHz for a 40°–15°–8° impedance transformer, with $R_s = 0.5$ Ω.

https://doi.org/10.1017/S175907870999050X Published online by Cambridge University Press

load" are very different compared to the results with $R_s = 1.6\ \Omega$ (Fig. 14).

To bring to the fore the importance of the "matching load" method, we can compare Fig. 15(a) with Fig. 13 ($R_s = 0.5\ \Omega$) and Fig. 14(a) with Fig. 13 ($R_s = 1.5\ \Omega$). These results obtained with the same varactors give totally different covered area. So an important difference between the two different methods of simulation is clearly pointed out. We note that insertion loss is more critical for this topology ($\theta_1 = 40^\circ$, $\theta_2 = 15^\circ$, and $\theta_3 = 8^\circ$) than for the first topology ($\theta_1 = 15^\circ$, $\theta_2 = 15^\circ$, and $\theta_3 = 8^\circ$).

It is obvious that in the case of lossy varactors, i.e. the reality in most cases, the "matching load" method has to be used in order to calculate and optimize by simulation the different parameters as the electrical length and the characteristic impedance of each transmission line, in order to achieve a maximum covered area in the Smith chart.

IV. PROTOTYPE DESIGN

To demonstrate the principles developed in Sections II and III, a tunable impedance transformer proof of concept was designed for a 1-GHz working frequency. The circuit was optimized with a Mathematica program using the "matching load" method. Commercial varactors (M/A-COM^{TM} type MA4ST-1240) were used. Their $L_s = 1.8$ nH, $R_s = 1.6\ \Omega$, and $C_c = 0.11$ pF. The $C(V)$ range, extracted from experimental results, was 1.0–8.6 pF for a bias voltage V range from 12 to 0 V. Coplanar waveguide (CPW) was used, the prototype being fabricated on a Rogers^{TM} RO4003 substrate ($\varepsilon_r = 3.36$, $\tan(\delta) = 0.0035$, dielectric thickness 0.813 mm, and copper thickness 35 μm). The transmission-line characteristic impedance was set at 200 Ω, leading to a CPW central conductor width of 250 μm and a gap of 2.8 mm. Two varactors were used in parallel to realize the tunable capacitors. This is necessary for CPW symmetry and to lower effective series resistance.

The fabricated proof of concept is shown in Fig. 16. By providing an air gap in the ground plane, separate reverse biases V_1 and V_2 can be applied to the two pairs of diodes. Surface mounted capacitors were used to ensure ground continuity for the RF signal.

The overall electrical length was 38° ($\theta_1 = 15^\circ$, $\theta_2 = 15^\circ$, and $\theta_3 = 8^\circ$), corresponding to $\sim\lambda/10$. The effective ε_r was 1.75, leading to $l_1 = 9.4$ mm, $l_2 = 9.4$ mm, and $l_3 = 5$ mm.

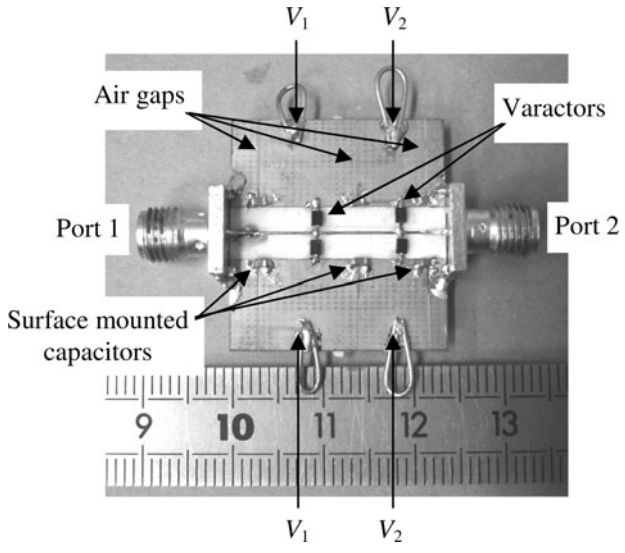

Fig. 16. Photograph of the impedance transformer.

V. RESULTS

In this section, the simulated and measured results obtained by the two methods are compared.

In Subsection A, the tunable frequency range of the impedance transformer loaded by 50 Ω is shown. In Subsections B and C, the simulated and measured results obtained from the "synthesized impedance" and "matching load" methods are compared.

For the simulations, lossless transmission lines were assumed but all parasitic elements of the diodes were considered. Measurements were made using a Wiltron 360 vector network analyzer (VNA).

A) Tunable frequency range for a 50-Ω load

An initial measurement using a 50-Ω load was made to extract the tunable bandwidth and to confirm the varactor's equivalent electrical model.

Figure 17 shows the frequency tunability of the complex-impedance transformer. Simulated and measured results for the parameters S_{11} and S_{21}, obtained for the extreme tunable frequencies, are shown. These correspond to the extreme capacitances of the variable capacitors. These results show that the transformer can be continuously tuned from 0.6 to 1.6 GHz, that is, ±60% around 1 GHz, with $|S_{11}| < -20$ dB and $|S_{21}| > -2$ dB. Good agreement between simulated and measured results was obtained for the whole tunable frequency range.

B) "Synthesized impedance" method

In the experimental setup shown in Fig. 18, the impedance transformer was inserted between the two ports of the VNA, and a coaxial SOLT (short-open-load-through) calibration procedure was applied between the calibration plans P_1 and P_2. The S_{22} parameter was measured at the impedance transformer output. The phase shift φ due to the SMA connector

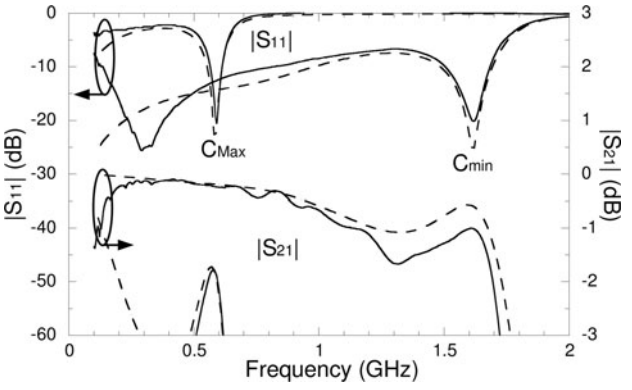

Fig. 17. Simulated (––) and measured (—) frequency tuning ranges for a fixed 50-Ω load.

https://doi.org/10.1017/S175907870999050X Published online by Cambridge University Press

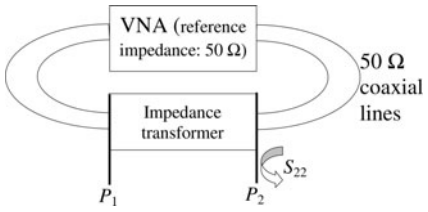

Fig. 18. Experimental setup for the measurement of S_{22}.

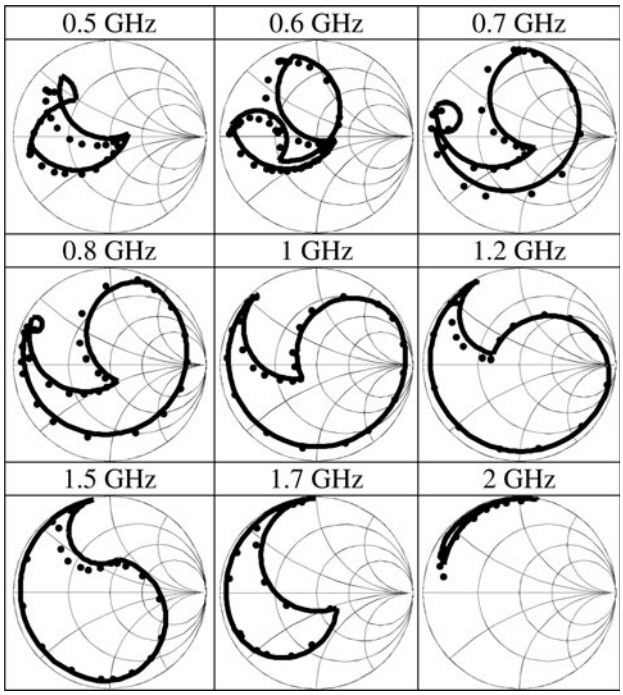

Fig. 19. Simulated S_{22} values (▬) compared with measured results (•••).

used in the prototype of Fig. 16 is given by

$$\varphi = -15.55f, \tag{9}$$

where f is the frequency in GHz. This phase shift is taken into account in measurement results.

Figure 19 compares the simulated and measured results from 0.5 to 2 GHz. The conditions are the same as in Fig. 6, with one varactor bias being fixed at its minimum or maximum value and the other being varied over its full range.

The tunable S_{22} area changes with the working frequency, and maximum coverage was obtained between 1.0 and 1.2 GHz. A good agreement between simulations and measurements was obtained for all frequencies.

The area of impedances covered by our device is comparable to best results obtained in the literature [10, 21] measured in this way, with a 50 Ω load. However, our device is much more simpler.

C) "Matching load" method

With the two criteria $|S_{11}| < -20$ dB and $|S_{21}| > -2$ dB, Fig. 20 shows the simulation results obtained when the operating frequency was varied from 0.5 to 2.0 GHz.

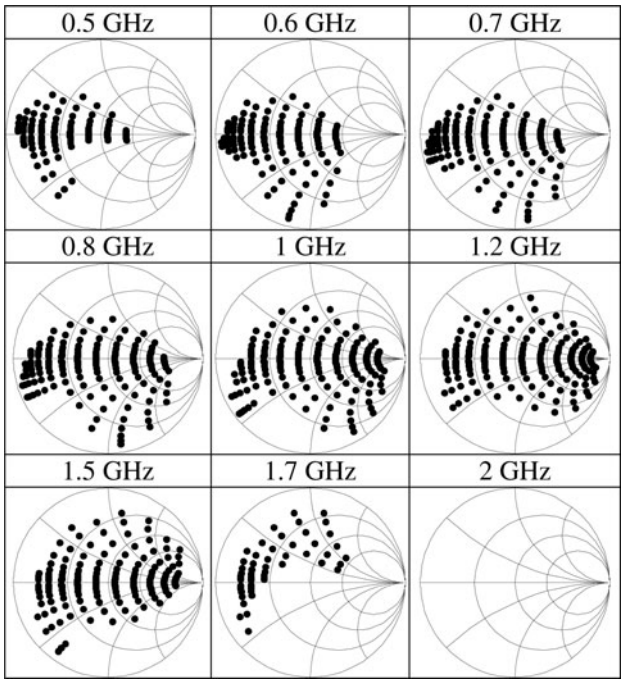

Fig. 20. Simulation results for the "matching loads" method with the criteria $|S_{11}| < -20$ dB and $|S_{21}| > -2$ dB versus frequency.

Measurements were carried out using an experimental approach similar to that used for the simulations. A mechanical tuner [28] was used as a complex load for the tunable impedance transformer under test. The measurement steps for the calibration are detailed in Fig. 21. First, a coaxial

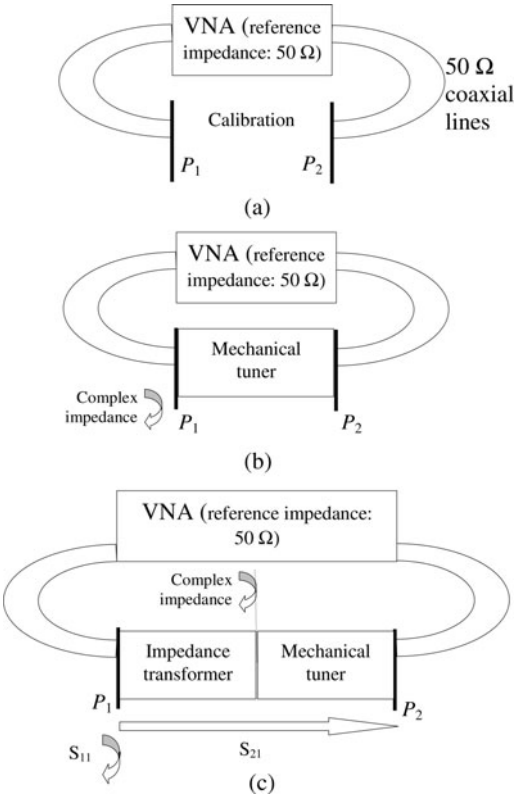

Fig. 21. Principle of the setups for the measurement of S_{11} and S_{21}: (a) calibration planes, (b) load impedance measurement, and (c) measurement of S parameters.

https://doi.org/10.1017/S175907870999050X Published online by Cambridge University Press

SOLT calibration was used to define reference plans P_1 and P_2 (see Fig. 21(a)). Then the input impedance of the mechanical tuner was measured, as shown in Fig. 21(b). Finally, the $|S_{11}|$ and $|S_{21}|$ parameters of the tunable transformer, loaded by the mechanical tuner, were measured (see Fig. 21(c)). We assume that the insertion loss of the mechanical tuner was negligible for the extraction of the insertion loss $|S_{21}|$ of the impedance transformer. The phase shifts of the SMA connectors are taken into account in measurement results.

The measured results are shown in Fig. 22 for three different frequencies: 0.8, 1.0, and 1.5 GHz. The lowest frequency was 0.8 GHz owing to the limited mechanical tuner bandwidth. The Smith charts show all the points for which the criteria $|S_{11}| < -20$ dB and $|S_{21}| > -2$ dB were satisfied. Each of these complex loads was associated with a pair of bias voltages (V_1, V_2), corresponding to two varactor capacitance values (C_{v1}, C_{v2}).

As this measurement procedure is much more time consuming than the "synthesized impedance" method, fewer measured load points were obtained, resulting in a "matching area" that is not so well defined as the simulated area.

The agreement between the measured results of Fig. 22 (a, b, c) and the simulated points in Fig. 22 (d, e, f) is good. The measurements show a large "matching area" that is slightly smaller than the simulated area.

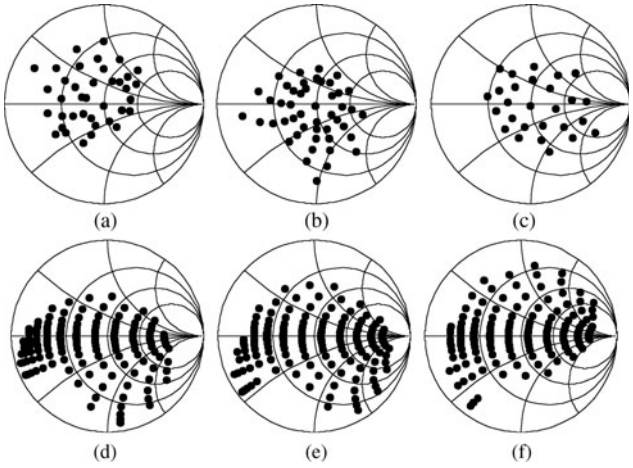

Fig. 22. Measured matched complex loads, under the conditions $-|S_{11}| < -20$ dB and $|S_{21}| > -2$ dB, at three frequencies: (a) 0.8 GHz, (b) 1.0 GHz, and (c) 1.5 GHz. Simulations extracted from Fig. 20 in the same conditions: (d) 0.8 GHz, (e) 1.0 GHz, and (f) 1.5 GHz.

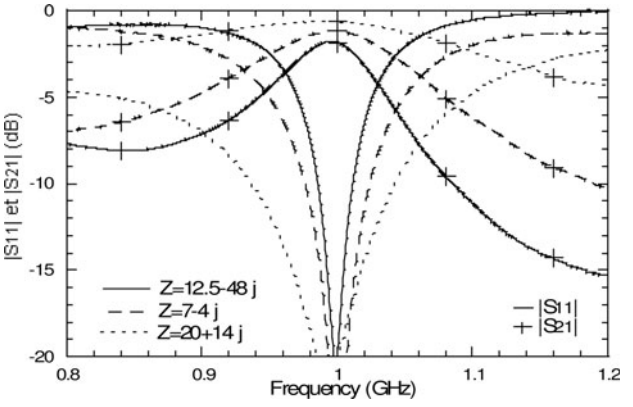

Fig. 23. Measured results for three different complex loads at 1 GHz, with the criteria $|S_{11}| < -20$ dB and $|S_{21}| > -2$ dB.

Figure 23 shows typical measured results obtained at 1 GHz for three different complex loads.

Conclusions and prospects: We believe that the totality of the results presented here validates our approach to both the design and the measurement methods.

VI. CONCLUSIONS

A principle for designing a compact tunable impedance transformer, based on a single transmission line loaded by only two pairs of varactors, has been proposed. The length of the transformer is only $\lambda/10$. A prototype with a 1 GHz center working frequency has been realized using commercial varactor diodes.

A good agreement has been obtained between the simulations and measurements and, as expected, the network provided a large coverage of the Smith chart (real part from 20 to 90 Ω at 0.8 GHz and from 30 to 170 Ω at 1.5 GHz), with a range of tunable working frequencies over ±40%.

Two different approaches to the design and measurements have been investigated. It is shown that an external tuner is necessary for accurate determination of the Smith chart coverage.

A MMIC prototype, in a 0.35 μm BiCMOS technology, is under development. It is believed that such an impedance transformer can be a good candidate for tunable matching of an amplifier embedded in a reconfigurable front-end.

ACKNOWLEDGEMENT

This work was supported by the Région Rhône-Alpes.

REFERENCES

[1] Sun, Y.; Fidler, J.K.: Design of Π impedance matching networks. IEEE Int. Circuits Syst. Symp., **5** (1994), 5–8.

[2] Hirota, T.; Minakawa, A.; Muraguchi, M.: Reduced-size branch-line and rat-race hybrids for uniplanar MMIC's. IEEE Trans. Microwave Theory Tech., **38** (3) (1990), 125–131.

[3] Bischof, W.: Variable impedance tuner for MMIC's. IEEE Microwave Guided Wave Lett., **4** (6) (1994), 172–174.

[4] Collins, C.E.; Pollard, R.D.; Miles, R.E.: A novel MMIC source impedance tuner for on-wafer microwave noise parameter measurements, In IEEE Microwave and Millimeter-Wave Monolithic Circuits Symp. Dig., 1996, 123–126.

[5] McIntosh, C.E.; Pollard, R.D.; Miles, R.E.: Novel MMIC source-impedance tuners for on-wafer microwave noise-parameter measurements. IEEE Trans. Microwave Theory Tech., **47** (2) (1999), 125–131.

[6] Sinsky, J.H.; Westgate, C.R.: Design of an electronically tunable microwave impedance transformer, In IEEE MTT-S Int. Microwave Theory Tech. Symp. Dig., 1997, 647–650.

[7] Jung, S.; Kan, K.; Park, J.H.; Chung, K.W.; Kim, Y.K.; Kwon, Y.: Micromachined frequency-variable impedance tuners using resonant unit cells, In IEEE MTT-S Int. Microwave Theory Tech. Symp. Dig., 2001, 333–336.

[8] Kim, H.T.; Jung, S.; Kang, K.; Park, J.H.; Kim, Y.K.; Kwon, Y.: Low-loss analog and digital micromachined impedance tuners at

https://doi.org/10.1017/S175907870999050X Published online by Cambridge University Press

the Ka-band. IEEE Trans. Microwave Theory Tech., **49** (12) (2001), 2394–2400.

[9] De Mingo, J.; Valdovinos, A.; Crespo, A.; Navarro, D.; Garcia, P.: An RF electronically controlled impedance tuning network design and its application to an antenna input impedance automatic matching system. IEEE Trans. Microwave Theory Tech., **52** (2) (2004), 489–497.

[10] Vaha-Heikkila, T.; Varis, J.; Tuovinen, J.; Rebeiz, G.M.: A 20–50 GHz RF MEMS single-stub impedance tuner. IEEE Microwave Wireless Compon. Lett., **15** (4) (2005), 205–207.

[11] Lange, K.L.; Papapolymerou, J.; Goldsmith, C.L.; Malczewski, A.; Kleber, J.: A reconfigurable double-stub tuner using MEMS devices, In IEEE Int. Microwave Theory Tech. Symp. Dig., Vol. **1**, 2001, 337–340.

[12] Papapolymerou, J.; Lange, K.L.; Goldsmith, C.; Malczewski, A.; Kleber, J.: Reconfigurable double-stub tuners using MEMS switches for intelligent RF front-ends. IEEE Trans. Microwave Theory Tech., **51** (1) (2003), 271–278.

[13] Zheng, G.; Kirby, P.L.; Pajic, S.; Pothier, A.; Papapolymerou, J.; Popovic, Z.: A monolithic reconfigurable tuner with ohmic contact MEMS switches for efficiency optimization of X-band power amplifiers, In Topical Meeting on Silicon Monolithic Integrated Circuits in RF Systems, 2004, 159–162.

[14] Vaha-Heikkila, T.; Varis, J.; Tuovinen, J.; Rebeiz, G.M.: A reconfigurable 6–20 GHz RF MEMS impedance tuner, In IEEE Int. Microwave Theory Tech. Symp. Dig., 2004, 729–732.

[15] Watley, R.B.; Zhou, Z.; Medle, K.L.: Reconfigurable RF impedance tuner for match control in broadband wireless devices. IEEE Trans. Antennas Propagat., **54** (2) (2006), 470–478.

[16] Qiao, D.; Molfino, R.; Lardizabal, S.M.; Pillans, B.; Asbeck, P.M.; Jerinic, G.: An intelligently controlled RF power amplifier with a reconfigurable MEMS-varactor tuner. IEEE Trans. Microwave Theory Tech., **53** (3) (2005), 1089–1095.

[17] Jrad, A.; Perrier, A.L.; Bourtoutian, R.; Duchamp, J.M.; Ferrari, P.: Design of an ultra compact electronically tunable microwave impedance transformer. Electron. Lett., **41** (12) (2005), 777–709.

[18] Jeong, H.T.; Kim, J.E.; Chang, I.S.; Kim, C.D.: Tunable impedance transformer using a transmission line with variable characteristic impedance. IEEE Trans. Microwave Theory Tech., **53** (8) (2005), 2587–2593.

[19] Chun, Y.H.; Hong, J.S.: Variable Zc transmission line and its application to a tunable impedance transformer, in 35th European Microwave Conf., 2005, 893–896.

[20] Shen, Q.; Barker, N.S.: A reconfigurable RF MEMS based double slug impedance tuner, in 35th European Microwave Conf., Paris, 2005, 537–540.

[21] Lu, Y.; Katehi, L.P.B.; Peroulis, D.: A novel MEMS impedance tuner simultaneously optimized for maximum impedance range and power handling, In IEEE Int. Microwave Theory Tech. Symp. Dig., Long Beach, 2005, 927–930.

[22] Vaha-Heikkila, T.; Rebeiz, G.M.: A 20–50 GHz reconfigurable matching network for power amplifier applications, In IEEE Int. Microwave Theory Tech. Symp. Dig., Forth Worth, Vol. **2**, 2004, 717–721.

[23] Pienkowski, D.; Wiatr, W.: Broadband electronic impedance tuner, in 14th Int. Conf. Microwaves Radar and Wireless Communications, Mikon, Vol. **1**, 2002, 310–313.

[24] Perrier, A.L.; Ferrari, P.; Duchamp, J.M.; Vincent, D.: A varactor tunable complex impedance transformer, in 34th European Microwave Conf., Amsterdam, Netherlands, Vol. **1**, 2004, 301–303.

[25] Pistono, E.; Perrier, A.L.; Bourtoutian, R.; Kaddour, D.; Jrad, A.; Duchamp, J.M.; Duvillaret, L.; Vincent, D.; Vilcot, A.; Ferrari, P.: Hybrid tunable microwave devices based on Schttky–Diode varactors. Proc. Eur. Microwave Assoc. (Special issue on Front'end Solution Cell. Commun. Terminals), **12** (2005), 109–116.

[26] Mathematica, version 4.0.

[27] Frickey, D.A.: Conversions between S, Z, Y, h, ABCD and T parameters which are valid for complex source and load impedance. IEEE Trans. Microwave Theory Tech., **42** (2) (1994), 205–211.

[28] Programmable Tuner, Focus Microwaves, 1808–2C model.

APPENDIX

Figure 24 shows a simplified *RC* equivalent circuit of a single varactor diode inserted between a source impedance Z_{in} and an output load impedance Z_{out}.

We denote Zs_{in} the input impedance as seen from Z_{in}. In admittance form this is

$$Ys_{in} = \frac{1}{Zs_{in}} = \frac{1}{R_s + \left(1/jC\omega\right)} + \frac{1}{\mathrm{Re}(Z_{out}) + j\,\mathrm{Im}(Z_{out})},$$

where $Z_{out} = \mathrm{Re}(Z_{out}) + j\mathrm{Im}(Z_{out})$. The input can be matched when Zs_{in} and Z_{in} are complex conjugates, that is when $Zs_{in} = Z_{in}{}^*$, or equivalently, $Ys_{in} = Y_{in}{}^*$, leading to

$$\frac{1}{R_s + (1/jC\omega)} + \frac{1}{\mathrm{Re}(Z_{out}) + j\,\mathrm{Im}(Z_{out})} = \frac{1}{\mathrm{Re}(Z_{in}) - j\,\mathrm{Im}(Z_{in}),}$$

where $Z_{in} = \mathrm{Re}\,(Z_{in}) + j\mathrm{Im}\,(Z_{in})$. Thus the output admittance that can be matched is

$$Y_{out} = \frac{1}{\mathrm{Re}(Z_{out}) + j\mathrm{Im}(Z_{out})} = \frac{1}{-R_s - \left(1/jC\omega\right)} + \frac{1}{\mathrm{Re}(Z_{in}) - j\mathrm{Im}(Z_{in})}$$

This corresponds to the impedance determined from the measurement of S_{11} and S_{21}, as shown in Subection IIIB.

Let us now calculate the output admittance Ys_{out} as seen from Z_{out}, as shown in Fig. 25. This is the impedance that is extracted from the measurement of S_{22}, as in Subection IIIA:

$$Y_{s_{out}}{}^* = \frac{1}{Z_{s_{out}}{}^*} = \frac{1}{R_s - (1/jC\omega)} + \frac{1}{\mathrm{Re}(Z_{in}) - j\,\mathrm{Im}(Z_{in})}.$$

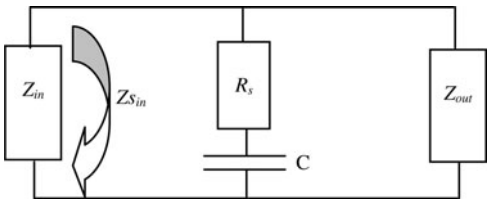

Fig. 24. Input impedance Zs_{in} seen from Z_{in}.

https://doi.org/10.1017/S175907870999050X Published online by Cambridge University Press

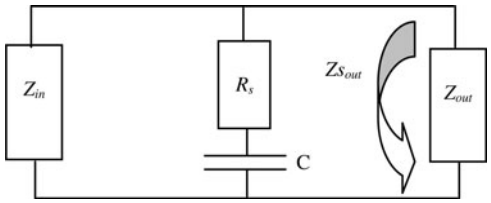

Fig. 25. Output impedance Zs_{out} seen from Z_{out}.

At this point, it becomes obvious that Y_{out} and Ys_{out}^* are different. This is because R_s is not equal to zero. These equations explain why the two measurement approaches investigated in Subections IIIA and B do not lead to the same results when the series resistance of the varactors is considered.

Anne-Laure Perrier was born in France in 1980. She received the M.Sc. degree in Optics, Optoelectronics, and Microwaves from the INPG ("Institut National Polytechnique de Grenoble"), Grenoble, France, in 2003. She received the Ph.D. degree in 2006 from the Laboratory of Microwaves and Characterization (LAHC), University of Savoie, France. Her research interests include the theory, design, and realization of tunable-impedance transformers.

She has been an Assistant Professor since September 2008 at Claude Bernard University (Lyon, France), where she teaches electronics and signal processing. She continues her research at the Research Center on Medical Imaging (Creatis-LRMN). She designs and realizes RF sensors for MRI (Magnetic Resonance Imaging) applications.

Jean-Marc Duchamp was born in Lyon, France, on April 10, 1965. He received the M.Sc. degree from the University of Orsay, (France), in 1988 and the Engineer degree in 1990 from Supelec. He has been a Research Engineer at Techmeta (France) from 1991 to 1996. He received the Ph.D. degree in 2004 from LAHC, University of Savoie (France). He has been an Assistant Professor since 2005 at J. Fourier University (Grenoble, France), where he teaches electronics and telecommunications. His current research interests include the analysis and design of nonlinear microwave and millimeter-wave circuits, such as nonlinear transmission lines, periodic structures, and tunable impedance transformers.

Olivier Exshaw was born in France in 1973. He received the Engineer degree in the field of microelectronics from ENSERG/INPG, Grenoble, France, in 2003. He was with the Ultra-High-Frequency and Optoelectronic Characterization Laboratory until the end of 2005. From 2006, he has been Electronic Service Project Manager at the Research Center for Very Low Temperatures (CRTBT) at CNRS.

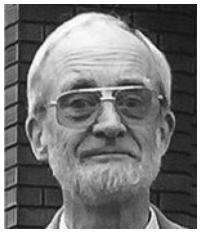

Robert G. Harrison (M'82) received the B.A. and M.A. (Eng.) degrees from Cambridge University, UK, in 1956 and 1960, respectively, and the Ph.D. and D.I.C. degrees from the University of London, UK, in 1964.

From 1964 to 1976, he was with the Research Laboratories of RCA Ltd., Ste-Anne-de-Bellevue, QC, Canada, In 1977, he became Director of Research at Com Dev Ltd., Dorval, QC, where he worked on nonlinear microwave networks. From 1979 to 1980, he designed spread-spectrum systems at Canadian Marconi Company, Montreal, QC, Canada. From 1980, he has been a Professor in the Department of Electronics, Carleton University, Ottawa, ON, Canada. His research interests include the modeling of nonlinear microwave device/circuit interactions by a combination of analytical and numerical techniques. More recently, he has been developing new analytical models of ferromagnetic phenomena based on both quantum-mechanical and classical physics. He has authored or coauthored more than 60 technical papers, mostly in the area of nonlinear microwave circuits, as well as several book chapters on microwave solid-state circuit design. He holds several patents on microwave frequency-division devices. He became a Distinguished Research Professor of Carleton University in 2005.

Dr. Harrison received the "Inventor" award from Canadian Patents and Development in 1978.

Philippe Ferrari was born in France in 1966. He received the B.Sc. degree in Electrical Engineering in 1988 and the Ph.D. degree from the INPG ("Institut National Polytechnique de Grenoble"), France, in 1992.

From September 2004, he has been a Professor at the University Joseph Fourier at Grenoble, France, while he continues his research at the Institute of Microelectronics, Electromagnetism, and Photonics (IMEP) at INPG.

His main research interest is the design and realization of tunable and miniaturized RF and millimeter wave devices, transmission lines, filters, phase shifters, power dividers, tuners, in PCB and RFIC technologies.

He is also involved in the development of time-domain techniques for the measurement of passive microwave devices and for soil moisture content.

https://doi.org/10.1017/S175907870999050X Published online by Cambridge University Press